Pion absorption on ^{4}He into the ppd final state

M. Planinić,[8] D. Androić,[8] G. Backenstoss,[1] D. Bosnar,[8] T. Dooling,[6] M. Furić,[8] P. A. M. Gram,[3] N. K. Gregory,[4] A. Hoffart,[2,7] C. H. Q. Ingram,[7] A. Klein,[6] K. Koch,[7] J. Köhler,[1] B. Kotliński,[7] M. Kroedel,[1] G. Kyle,[5] A. Lehmann,[1,7] A. O. Mateos,[4] K. Michaelian,[7] T. Petković,[8] R. P. Redwine,[4] D. Rowntree,[4] N. Simičević,[4] R. Trezeciak,[2] H. Ullrich,[2] H. J. Weyer,[1,7] M. Wildi,[1] and K. E. Wilson[4]

(LADS Collaboration)

[1]*University of Basel, CH-4056 Basel, Switzerland*
[2]*University of Karlsruhe, D-7500 Karlsruhe, Germany*
[3]*LAMPF, Los Alamos, New Mexico 87545*
[4]*Massachusetts Institute of Technology, Cambridge, Massachusetts 02139*
[5]*New Mexico State University, Las Cruces, New Mexico 88003*
[6]*Old Dominion University, Norfolk, Virginia 23529*
[7]*Paul Scherrer Institute, CH-5232 Villigen PSI, Switzerland*
[8]*University of Zagreb, HR-10000 Zagreb, Croatia*

(Received 7 October 1999; published 5 April 2000)

Results from a 4π solid angle measurement of the reaction $\pi^+ + {}^4\mathrm{He} \rightarrow ppd$ at incident pion energies of $T_{\pi^+} = 70$, 118, 162, 239, and 330 MeV are presented. Integrated cross sections are given for the final states with energetic deuterons (ppd) and $(pd)p$. The differential cross sections are described by a complete set of five independent variables and various other kinematic variables and compared to cascade and phase space models where deuterons were formed by a semiclassical pickup model. The data are investigated for signatures of initial and final state interactions: it is found that more than half of the (ppd) yield cannot be explained by these mechanisms. The remaining strength is reasonably well reproduced by $3N$ phase space models followed by pickup.

PACS number(s): 25.80.Ls, 25.10.+s

I. INTRODUCTION

Pion absorption on a free nucleon does not occur since energy and momentum cannot be conserved. In the $\Delta(1232)$ resonance region most of the total pion absorption strength in systems with few nucleons comes from the two nucleon absorption (2NA) quasideuteron mode. However, several experiments on light nuclei [1–13] have reported that a significant fraction of the absorption cross section is due to events in which the energy of the absorbed pion is shared between three or more particles. Particularly, some small solid angle experiments on ^{3}He in the Δ resonance region have reported that the energy distribution of about one quarter of the absorption cross section appeared consistent with three-nucleon phase space [1–5].

The absorption reaction of a pion on a nucleus has often been subdivided into a genuine absorption part and into secondary modifications (such as rescattering processes) due to the surrounding nuclear medium. Recent large solid angle measurements of the pion absorption cross section on the few body systems [13–15] have reported that there is a significant, but not dominant, contribution to the three nucleon absorption (3NA) cross section from a process in which the pion initially interacts with one of the nucleons [initial state interaction (ISI)] before being absorbed on a deuteronlike pair. Another cascade process would be 2NA followed by a nucleon-nucleon interaction [final state interaction (FSI)]. However, no clear signal of that process has been seen in the helium isotopes [12,15]; recent Faddeev-type calculations [16] also suggest it should not have a large probability.

Although investigation of pion absorption on ^{3}He has given some important insight into 3NA, a more interesting case is ^{4}He. The presence of an additional nucleon opens up additional physics channels which can compete with the 3NA process, and yet the system is still simple enough that the experimental kinematics can be completely determined for most of the final states. There are two significant final states for π^+ absorption on ^{4}He $pppn$ and ppd. Results of a detailed investigation of the cross sections and distributions of the first one have been published recently [17,18], but the second one, the ppd, remained less well investigated. In the work of Mateos *et al.* [17], ppd distributions were reported to show some indications that after pion absorption a pickup of a neutron or proton, by one of the outgoing nucleons, could follow, thus forming the ppd final state. However, for such conclusions more detailed comparisons with models are needed. Therefore the investigation of the distributions of the ppd state is necessary to complete our knowledge about the 3NA pion absorption mode in ^{4}He.

In this paper all models leading to energetic final state deuterons explicitly assume a pick-up mechanism to form the deuteron. Other approaches could be used for some channels, such as using a quasifree $\pi^+ + t \rightarrow p + d$ cross section as input (see Ref. [19], for example). It turns out, however, that the pickup mechanism reproduces the $\pi^+ + t \rightarrow p + d$ angular distributions rather well (see Sec. IV C) bringing the two models close to equivalency. In any realistic model the deuteron form-factor imposed on an underlying *p*-wave distribution will be a dominating influence on the deuteron distributions (as is indeed apparent in the data).

In the present paper we report results of pion absorption on ^{4}He into the ppd final state. Data at five incident positive pion energies (70, 118, 162, 239, and 330 MeV) were measured with a 4π solid angle detector. Some of the results have been reported earlier [17,18]. Distributions will be compared to different models which include pickup by one of the outgoing nucleons.

II. EXPERIMENT

The experiment was performed at the $\pi M1$ channel at the Paul Scherrer Institute (PSI) in Villigen, Switzerland with the Large Acceptance Detector System (LADS) [20,21] which was designed to study multinucleon pion absorption.

There are two characteristics of LADS which combined make an important improvement compared to previous pion absorption experiments. These are the solid angle coverage of the detector of 98% of 4π and the low detection threshold energy $T_{\rm thr}\approx 20$ MeV for protons and $T_{\rm thr}\approx 30$ MeV for deuterons. Thus, only small extrapolations of the measured distributions are needed. The detector was cylindrical in shape with an active volume of 1.6 m length. It was divided into 28 ΔE-E-E plastic scintillator sectors, read out at both ends, and two 14 sector ΔE-E ''end-cap'' blocks to close the cylinder. The scintillators stopped normally incident protons of up to 250 MeV. Two coaxial cylindrical wire chambers provided tracking information for charged particles with an angular resolution of about 1° and a vertex resolution of less than 2.5 mm full width at half maximum (FWHM). The target used in the experiment consisted of a 4 cm diameter, 25.7 cm long carbon fiber cell, with walls of 0.5 mm thickness to keep background and particle threshold low, containing ^{4}He at a pressure of 100 bar.

The incident π^+ beam was defined using plastic scintillator detectors which counted individual pions; these were identified by time-of-flight and pulse height analysis. From a total incident flux of about 3×10^6/sec, a beam rate of about 1×10^5/sec was accepted by a 2 cm diameter scintillator placed about 50 cm upstream of the target center.

Events were classified in the trigger logic according to the number of charged and neutral particles detected in LADS in coincidence with a valid incident pion. The various event types were then prescaled individually according to the physics interest of the information they contained.

III. DATA ANALYSIS

A. Treatment of raw data

The reconstructed interaction vertex position was used to eliminate events from the target end walls, using the trajectory information measured by the multiwire proportional chambers (MWPCs). Only events with track information for all charged particles, a vertex within 10 cm upstream and downstream of the target center and within 1.7 cm of the beam axis were accepted. Vertex reconstruction plots can be found in Ref. [15].

For the separation of protons and deuterons from pions and other particles conventional E-dE/dx and E-TOF (time-of-flight) particle identification (PID) techniques were applied (see Fig. 4 in Ref. [15]). The latter was used for all charged particles with less than 10 MeV light deposited in the E scintillators, because these were stopped in or just passed through the thin ΔE counters. Figure 1 illustrates the p-d separation when using the E-dE/dx technique.

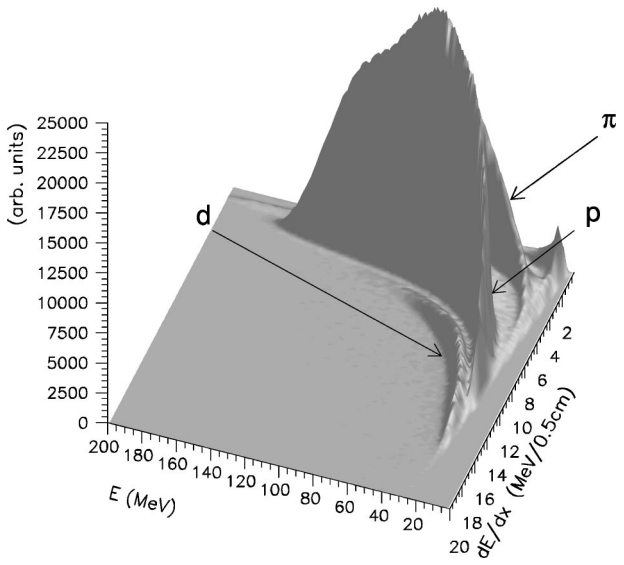

FIG. 1. E-dE/dx spectra used for particle identification showing the p-d separation. The pion energy is $T_\pi=118$ MeV and the reaction is ^{4}He(π^+,x).

In the next step only events with deuterons and protons but with no identified charged pion were selected. A cut on the reconstructed missing mass of ± 20 MeV around the peak center removed most of the background events originating from remaining pionic final states, mainly due to single charge exchange, which are separated by about the pion mass. Furthermore, most events where a proton underwent a nuclear reaction in the scintillator material and lost a part of its energy were rejected by this cut.

In the analysis of the deuteronic final states, a significant problem is the possibility of misidentifying a proton as a deuteron since there are many more of the former. In order to determine the probability of mistakenly identifying a proton as a deuteron or a proton as a pion, data were used from the interaction of 330 MeV π^+'s with ^{3}He and the method of Ref. [22]. The probability for a proton to be misidentified as a deuteron was determined as a function of proton energy. It was between 2 and 3% for proton energies above 40 MeV but rose to up to 11% for low energy protons. The probability for a proton to be mistakenly identified as a pion rose smoothly from 0% at low energy to above 11% above 200 MeV. For the ^{4}He data most of the events where protons were misidentified as deuterons were later removed by the reconstructed missing mass cut.

To eliminate events near the edge of the detector acceptance the polar angular range of the data was limited between 15° and 165°. With this cut the solid angle coverage was slightly reduced to 96.6% of 4π. For events with only two charged particles detected, this cut was further reduced to $20°-160°$.

B. Normalization

Once the absorption events were isolated, the measured raw counts were normalized to the number of incident pions

and target scatterers to yield a raw cross section. Corrections were made to the number of incident pions to account for contamination in the beam, for the number of pions lost through decay or reactions before reaching the target, and for pions missing the target. The largest systematic uncertainty in the determination of the normalization resulted from this last correction. It was measured by examining the radial distribution of events from the air upstream and downstream of the target, and the uncertainty in this correction ranged between 3 and 12 %. The number of target scatterers was determined from measurements of the pressure and temperature of the target. The areal density of the target was typically 4.5×10^{22} nuclei/cm^2, and was known with an uncertainty of 1%. In addition, a correction was applied for each trigger type to account for its prescale factor mentioned in Sec. II, to yield the raw cross section [23,24].

IV. MONTE CARLO SIMULATIONS AND FITS

A. Classification of events

In this paper we use the nomenclature that final state nucleons (deuterons) inside the round brackets participated in the reaction while those outside were spectators, independent of whether they were detected. This classification of a final state according to the particles which have participated in the absorption reaction is called the ''physics channel.'' On the other hand for the full decomposition of the ppd final state of ^{4}He into absorption mechanisms a classification into ''selected channels'' turned out to be useful. The purpose was to produce separate distributions for the physics channels $(pd)p$ and (ppd) to get more constraints for the fits. These selected channels were defined by the following classification scheme (note the use of square brackets to denote them):

$$
\begin{aligned}
&[pd]p\text{: } T_{p1}>30 \text{ MeV; } T_d>30 \text{ MeV; } T_{p2}\leqslant 30 \text{ MeV;}\\
&[ppd]\text{: } T_{p1}>30 \text{ MeV; } T_{p2}>30 \text{ MeV; } T_d>30 \text{ MeV;}\\
&[pp]d\text{: } T_{p1}>30 \text{ MeV; } T_{p2}>30 \text{ MeV; } T_d\leqslant 30 \text{ MeV.}
\end{aligned}
$$

The distributions $[pd]p$ and $[ppd]$ presented in this paper will always be with these thresholds on the laboratory kinetic energies T corrected for energy loss in the apparatus. To test the model dependence of the extrapolations of the cross sections down to zero threshold and their decompositions into mechanisms a data set with the same classification scheme, but a 20 MeV threshold, was also investigated. The variations in the results are reflected in the quoted uncertainties. Distributions of the $[pp]d$ selected channel will not be shown since the resolution of the missing mass in the experiment was not sufficient to separate events with a spectator deuteron from those with an unbound pn pair, as can be seen in Ref. [17].

B. Monte Carlo simulations

Monte Carlo simulations were made to correct for the acceptance and inefficiencies of the detector and to assist the physics interpretation of the data. For all simulations, the particles were tracked through a model of the detector using the CERN GEANT software package. The simulated data were then treated with the same analysis program as used for the real data. The experimental resolutions and hardware thresholds, as determined from the data for each scintillation counter and MWPC, were applied to the simulated raw events. The effects of geometrical acceptance, energy thresholds and reaction losses in the detector, as well as inefficiencies of the chambers and the reconstruction code, were thus reflected in the simulated particle distributions in the same way as in those of the experimental data. The reliability of this procedure was tested in many ways and is discussed in detail elsewhere [13,23].

TABLE I. Summary of event generators used to simulate the different absorption mechanisms of the reaction $\pi^+ + {}^4\mathrm{He}\rightarrow ppd$. More detailed descriptions of the abbreviations are given in the text. Each σ represents a differential cross section as a function of the polar scattering angle. The ρ_N represents a one-nucleon momentum density distribution, ρ_d represents a deuteron momentum density distribution, and F_{pick} the pickup weighting step function.

Event generator	Weighting factors
$4\mathrm{NA}_{(pppn)}+\mathrm{pickup}$	$4\mathrm{NA}_{pppn} * F_{\mathrm{pick}}$
$3\mathrm{NA}^{L\geqslant 0}_{(ppp)n}+\mathrm{pickup}$	$4\mathrm{NA}^*_{pppn}\rho^*_N P_0[\cos(\xi)]^* F_{\mathrm{pick}}$
$3\mathrm{NA}^{L\geqslant 1}_{(ppp)n}+\mathrm{pickup}$	$4\mathrm{NA}^*_{pppn}\rho^*_N\{1-P_2[\cos(\xi)]\}^* F_{\mathrm{pick}}$
$\mathrm{ISI}_{(ppp)n}+\mathrm{pickup}$	$\rho^*_N\rho^*_N\sigma_{\pi^+p\rightarrow\pi^+p}{}^*\sigma_{2\mathrm{NA}}{}^* F_{\mathrm{pick}}$
$\mathrm{HFSI}_{(ppp)n}+\mathrm{pickup}$	$\rho^*_N\rho^*_N\sigma_{2\mathrm{NA}}{}^*\sigma^*_{pp} F_{\mathrm{pick}}$
$2\mathrm{NA}_{(pp)d}$	$\rho^*_d\sigma_{2\mathrm{NA}}$
$2\mathrm{NA}_{(pd)p}$	$\rho^*_N\rho_N * \sigma_{2\mathrm{NA}}{}^* F_{\mathrm{pick}}$

For the reaction $\pi^+ + {}^4\mathrm{He}\rightarrow ppd$, seven different event generators were found to be necessary (see Table I). All of them were based on mechanisms of the 2NA, 3NA, and 4NA absorption modes, as found in our previous works [15,17,18], followed by the pickup of a neutron by one of the outgoing protons. This pickup model will be discussed in more detail in Sec. IV C. The seven event generators are described here.

In the quasifree 2NA model ($2\mathrm{NA}_{(pp)d}$) the absorption has been taken as occurring on a quasideuteron inside the ^{4}He nucleus, using Ritchie's parametrization [25] for absorption on a deuteron and a deuteron momentum distribution ρ_d calculated by Schiavilla [26]. Here the final state deuteron is treated as a spectator, and no pickup is involved.

In the quasifree 2NA+pickup model ($2\mathrm{NA}_{(pd)p}$) the absorption has been taken again to be the same as that on a free deuteron using Ritchie's parametrization [25] and weighted first with spectator proton and neutron momentum distributions ρ_N from Ref. [26], and then weighted with the additional pickup weighting as mentioned above. An alternative model has also been tested for the ($2\mathrm{NA}_{(pd)p}$) channel where the pion is absorbed on a quasitriton $^3\mathrm{H}(\pi^+,pd)$ with one proton acting as a spectator. For that purpose the differential cross section of pion absorption on a quasitriton has been taken from the Ref. [7] and weighted with spectator proton distribution as above. The distributions from both models were similar.

To model the one-step 3NA followed by pickup ($3NA^{L\geq 0}_{(ppp)n}$ + pickup, $3NA^{L\geq 1}_{(ppp)n}$ + pickup), the neutron in the $4N$ phase space distribution was weighted with a momentum distribution (ρ_N) from a calculation by Schiavilla [26] adjusted to fit the ^{4}He$(e,e'p)^3H$ data [27]. To take into account angular momentum effects [15,28] the events of this generator were additionally weighted by the Legendre polynomials $P_0[\cos(\xi)]$ ($3NA^{L\geq 0}_{(ppp)n}$) and $\{1-P_2[\cos(\xi)]\}$ ($3NA^{L\geq 1}_{(ppp)n}$); for the definition of ξ see Sec. IV D.

It was found, looking at the distributions from different variables, that it is impossible to distinguish between the two processes:

$$\pi^+ + {}^4\mathrm{He} \rightarrow (ppp)n \quad \text{followed by pickup} \rightarrow (ppd)$$

and

$$\pi^+ + {}^4\mathrm{He} \rightarrow (ppn)p \quad \text{followed by pickup} \rightarrow (ppd),$$

where it was assumed that the intermediate state is similar for the (ppp) and (ppn) cases (e.g., $3N$ phase space). That is the reason why $(ppn)p$ models, followed by pickup, were not included. While in principle the $(ppn)p$ pickup process can also have a term proportional to $P_1[\cos(\xi)]$, the fits without it appear to be adequate and the resulting analysis is consistent with that of Ref. [15]. The distributions of ($ISI_{(ppp)n}$ + pickup) and ($HFSI_{(ppp)n}$ + pickup) were generated by an incoherent superposition of the two elementary processes followed by pickup. In the ISI model the pion was first scattered by one proton, moving with Fermi momentum (ρ_N), according to the differential elastic πp cross section ($\sigma_{\pi^+ p\rightarrow\pi^+ p}$, calculated with SCATPI [29]), before being absorbed on a quasideuteron recoiling from the pn system with a momentum distribution of ($\rho_N^*\rho_N$), with the quasifree 2NA cross section (σ_{2NA}) [25]. A suppression of the forward pion quasielastic cross section was taken into account [15]. The other two ISI processes, a quasielastic scattering of the π^+ on a neutron ($\sigma_{\pi^+ n\rightarrow\pi^+ n}$) and a charge-exchange reaction of the type $\pi^+ n\rightarrow\pi^0 p$ ($\sigma_{\pi^+ n\rightarrow\pi^0 p}$), both followed by the actual quasifree absorption (σ_{2NA}) on a quasideuteron, were simulated as in Ref. [18] and found to have similar distributions as the first one. In the HFSI model the pion was first absorbed on a quasideuteron moving with Fermi momentum opposite to that of the recoiling pn system ($\rho_N^*\rho_N$), and then one of the outgoing protons was scattered off the recoil proton according to its differential elastic NN cross section (σ_{pp}), calculated with SAID [30] and with a minimum momentum transfer of 150 MeV/c. The second way of modeling the HFSI process was the same as above, except that in the second step one of the protons was scattered elastically off the neutron (σ_{pn}) which has picked up a spectator proton. The distributions of the second HFSI (including pickup) model were not distinguishable from the first one. For all these models, the pickup weight between all pn pairs was added as a third step.

To model four-nucleon absorption followed by pickup ($4NA_{(pppn)}$ + pickup), three protons and one neutron were generated with constant density in phase space ($4NA_{(pppn)}$) and then weighted with the pickup weighting function. It was also found that distributions of four-nucleon phase space followed by pickup and ppd phase space are similar and so the latter was also not included into the fitting procedure.

C. Pickup model

The pickup was represented by a simple step function depending on the relative momentum between a proton and the pickup neutron. For estimating the width of the step function the very simple approach of Ref. [31] was used, which consists of using classical kinematics in the nonrelativistic approximation. Because of the relative motion of the nucleons within a deuteron, their individual momenta at the instant of pickup are not simply one half of the deuteron's momentum $\vec{p}_d$. Rather, the proton was taken to have a momentum

$$\vec{p}_p = \frac{1}{2}\vec{p}_d \pm \vec{p}_0$$

and the neutron a momentum

$$\vec{p}_n = \frac{1}{2}\vec{p}_d \mp \vec{p}_0,$$

where $\vec{p}_0$ is the momentum associated with internal relative motion. Its magnitude is taken as the deuteron's Fermi momentum, about 70 MeV/c.

All combinations of pn pairs available after the absorption were weighted with the pickup weighting function. In most cases the lowest energy proton picks up the spectator neutron since that proton has the greatest chance to have its relative momentum within the step function.

In order to show that the pickup model is justified, a Monte Carlo simulation was made for the process ^{3}H(π^+,pd) and compared to the data from the Ref. [7]. Figure 2 shows that our model gives a reasonable description of the data. In the case of ^{4}He the distributions are also consistent with a model where the pion is absorbed on a quasitriton ^{3}H(π^+,pd) with one proton acting as a spectator.

D. Fits and efficiency correction

For the complete description of a three-body final state, five independent variables were used β, γ, ξ, $\psi_{\min}$, and $\psi_{\max}$, which have been introduced in Ref. [15]. The five variables listed above are calculated in the center of mass (c.m.) of these three particles. ξ and β are Euler angles describing respectively the angle between the normal to the three-particle plane and the incident beam and the azimuthal angle of that plane, while γ reflects the distribution of protons and deuteron within the plane; $\psi_{\min}$ and $\psi_{\max}$ are the minimum and maximum opening angles between pairs of the three particles.

The relative strength of the seven different physics processes were determined by simultaneous fits to kinematic distributions of the two selected channels $[pd]p$ and $[ppd]$, with the normalizations of the seven processes as free parameters of the fit. A more detailed description of the fitting

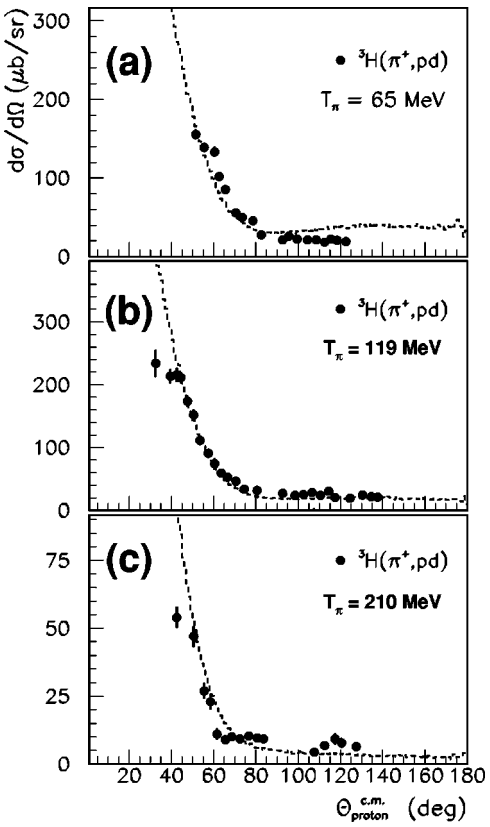

FIG. 2. The differential cross section $d\sigma/d\Omega$ of the reaction ^{3}H(π^+,pd) (the solid circles with error bars) from Ref. [7] compared to Monte Carlo simulations (dashed) of the pickup model for incident pion energies of 65 (a), 119 (b), and 210 MeV (c). The normalization of the Monte Carlo distributions is a free parameter.

procedure can be found in Refs. [15,18]. Fits were done to various histogram sets with the CERNLIB routine MINUIT: the five independent variables (β, γ, ξ, $\psi_{\min}$, $\psi_{\max}$), a set of selected one-dimensional distributions (proton polar angle θ_p, deuteron polar angle θ_d, proton kinetic energy T_p, deuteron kinetic energy T_d) and a set of two-dimensional histograms with pronounced correlations (θ_p vs p_p, θ_d vs p_d, m_x^2 vs p_p, m_x^2 vs p_d, m_x^2 vs θ_p, m_x^2 vs θ_d), where m_x^2 is defined in Refs. [13,32]. In addition, fits using all these distributions together were made.

The normalizations of some event generators had to be fixed, since due to the applied cuts and thresholds only small, but not negligible, spectator momentum tails contributed to the investigated ppd data sample. In these cases the contributing fractions were approximated from the partial cross sections, determined with the same data and published elsewhere [17]. These event generators were $2\mathrm{NA}_{(pp)d}$ and $2\mathrm{NA}_{(pd)p}$ for the $[ppd]$ selected channels.

The analysis was repeated with two different thresholds defining the selected channels. The average value obtained from the simultaneous fits with different histogram sets and thresholds was taken as the result for the contribution from each physics channel. The uncertainty associated with the fitting procedure was estimated from the variation of the results obtained under the different conditions. Using the results of the fit to define the relative strengths of the various models required to describe the raw data, these were then corrected for the acceptance and inefficiency of the detector using these Monte Carlo simulations.

In this paper, only the efficiency corrected histograms will be shown. The error bars of the data points in the histograms reflect the statistical uncertainties of the raw data and the simulations.

V. RESULTS

A. Partial absorption cross sections

The partial absorption cross sections for the deuteronic channels are presented in Table II. These cross sections are corrected for all detector inefficiencies, thresholds, and acceptance cuts. Except for the $(pd)p$ channel at 239 and 330 MeV the overall size of these corrections is roughly a factor of 2 (see also Ref. [17]). We have previously reported values for cross sections of the (ppd) and $(pd)p$ physics channels [17] but those presented here use more detailed models. The agreement between this work and our previous publication [17] obtained for the cross section of both channels is within the quoted uncertainties. Figure 3 shows a comparison of the deuteronic final state cross sections to cross sections from other ^{4}He pion absorption physics channels from Refs. [17,18]. The cross section attributable to the $(pd)p$ process falls steadily with increasing incident pion energy while the energy dependence of the (ppd) cross section shows a broad

TABLE II. Partial cross sections of the reaction $\pi^+ + {}^4\mathrm{He} \rightarrow ppd$, extrapolated to zero threshold, for the (ppd) and $(pd)p$ physics channels and with 30 MeV threshold for the protons and deuterons for the $[ppd]$ and $[pd]p$ selected channels. All cross sections are in mb. The given uncertainties reflect the normalization uncertainties and the systematic uncertainties due to the results of the different models and fits, added in quadrature.

T^{thr} (MeV)	Channel	70 (MeV)	118 (MeV)	162 (MeV)	239 (MeV)	330 (MeV)
0	$(pd)p$	3.0±0.4	2.6±0.2	1.7±0.2	0.7±0.1	0.2±0.1
0	(ppd)	1.5±0.2	3.2±0.6	4.7±0.7	1.5±0.1	0.7±0.1
30	$[pd]p$	2.4±0.2	2.2±0.1	1.5±0.1	0.6±0.1	0.2±0.1
30	$[ppd]$	0.37±0.05	0.85±0.07	1.3±0.1	0.60±0.05	0.29±0.04

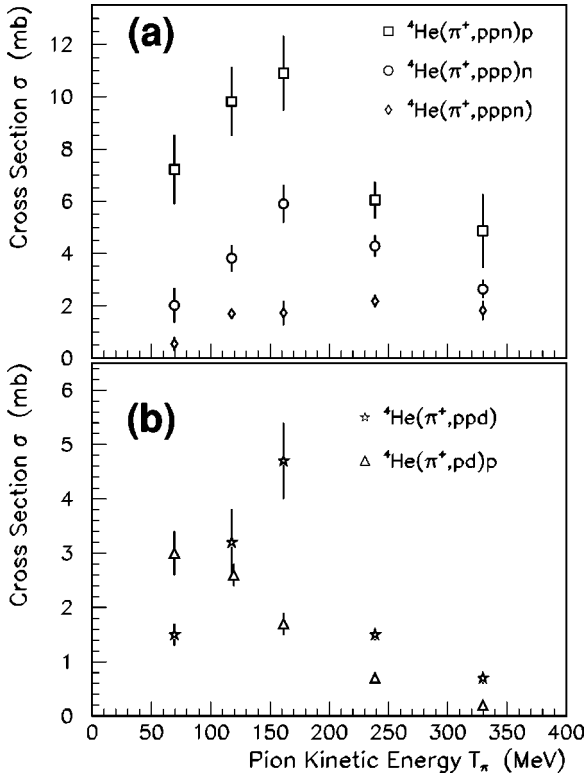

FIG. 3. (a) Decomposition of the $pppn$ absorption yield on ^{4}He according to the energetic final state particles (taken from Ref. [18]). (b) Cross sections of the ppd deuteronic final states.

resonancelike behavior peaking somewhere around 160 MeV. The contribution of the ppd final state to the total absorption cross section appears to fall as a function of energy from 13% at 70 MeV to 6% at 330 MeV.

With these results and those of Ref. [18] we were able to determine an estimate for the total pion absorption cross section at the incident pion kinetic energy of $T_{\pi^+}=330$ MeV, which we have not previously reported. We find $\sigma_{\rm abs}(330\ \text{MeV})=14.0\pm1.5$ mb. This cross section was determined assuming that $(pp)d/pn$ partial cross section can be estimated from the well known cross section of the reaction $\pi^+ + d \rightarrow pp$ by scaling it with the factor 2.5. The partial cross section for the $(pn)pp$ was extrapolated from Ref. [17] and all other partial cross sections were taken from Ref. [18].

B. Differential cross sections

The non-2NA cross section in the ppd final state consists primarily of contributions from the $(pd)p$ and (ppd) channels. In this section the acceptance corrected differential distributions will be shown for five incident pion energies for the $[ppd]$ selected channel and four incident pion energies for the $[pd]p$ channel. These distributions are intended to show the quality of the fits. The data will be compared to the summed contributions of the fitted models.

For the incident pion energy of 330 MeV the highest energetic protons after the absorption process were not stopped by the scintillators and their kinetic energy is underestimated [15]. These events are then removed by the missing mass cut. It was found [33] that this problem seriously affects the

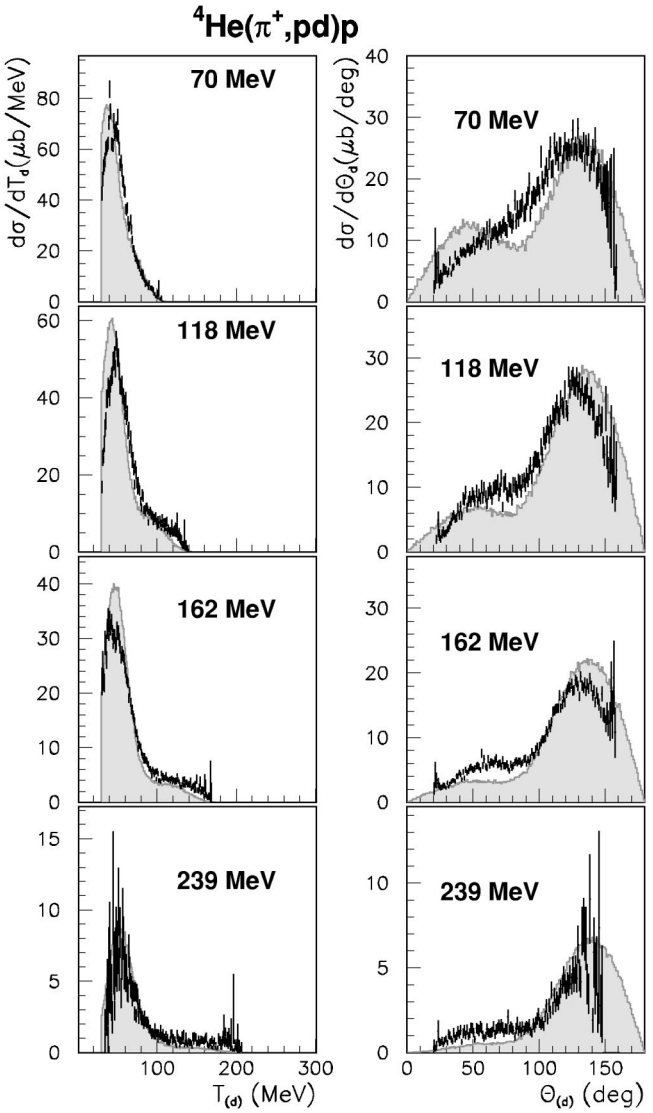

FIG. 4. The laboratory kinetic energy and polar angle distributions of the deuteron in the selected $[pd]$ channel (acceptance corrected) for incident pion energies of 70, 118, 162, and 239 MeV (from the top). The data are dots with error bars, the fitted sums of the simulations are the shaded areas. Normalization uncertainties are not included in the error bars.

distributions of the selected $[pd]p$ channel. However, the partial cross section can still be determined, and for distributions of the selected $[ppd]$ channel such losses were reliably taken into account by the Monte Carlo simulations. Therefore, for the highest incident pion energy only the distributions of the selected $[ppd]$ channel will be shown.

1. $(pd)p$ physics channel

Figures 4 and 5 show the energy and angular distributions of deuterons and protons in the selected $[pd]$ channel. The distributions of the $(pd)p$ channel are consistent with the deuteron resulting from pick-up by an outgoing nucleon, emerging preferentially at backward angles. The preference for the emission of the deuteron at backward angles can be qualitatively explained as being due to the smaller momen-

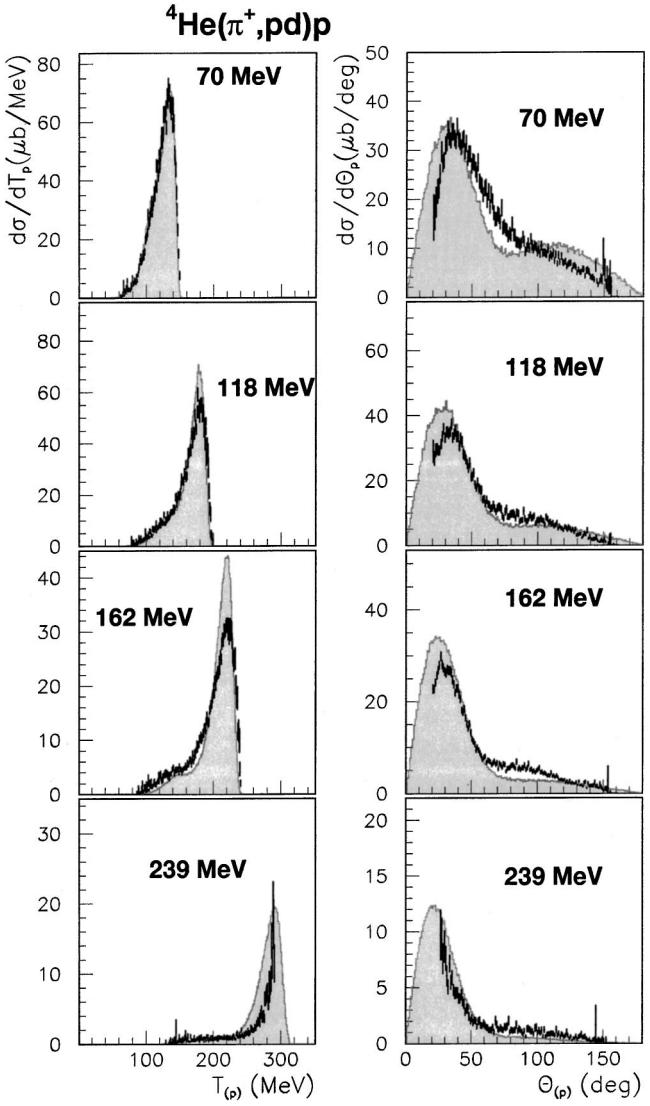

FIG. 5. The laboratory kinetic energy and polar angle distributions of the proton (acceptance corrected) in the selected $[pd]$ channel. For further information see Fig. 4.

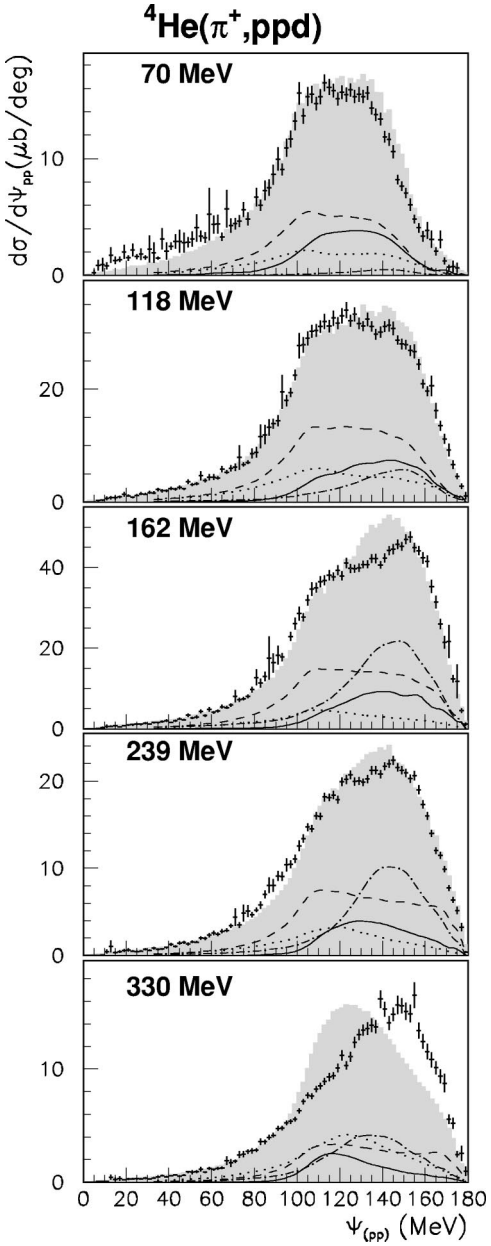

FIG. 6. pp-opening angle distributions in the laboratory frame (acceptance corrected) in the selected $[ppd]$ channel. The data (dots with error bars) were fitted with $2NA_{(pp)d}$ (solid line), $3NA_{(ppp)n}$+pickup (dashed), $ISI_{(ppp)n}$+pickup (dashed-dotted), $2NA_{(pd)p}$ (dotted), $HFSI_{(ppp)n}$+pickup (not shown), and $4NA_{(pppn)}$+pickup (not shown), as described in the text. The shaded areas are the sums of the fitted simulations. Normalization uncertainties are not included in the error bars.

tum transfer necessary for the pickup reaction at these angles. The main contribution comes from the $2NA_{(pd)p}$ model as described in Sec. IV B. The comparisons of the fits with the data show that the overall agreement is fair.

2. (ppd) *physics channel*

The low energy forward peaked behavior of the deuterons in the selected $[ppd]$ channel (see Fig. 8) suggests that the incoming pion initially scatters from a proton, which picks up a neutron to form a deuteron, while the pion is absorbed in the second step by the remaining pn pair. To further strengthen this argument one can look at the p-p opening angle in the lab system. If the deuteron really comes from the π-p process, then the $\pi^+ + d \rightarrow p + p$ should be undisturbed and one can see an opening angle signature around 160°. This is indicated in Fig. 6. A comparison of the data distributions with the ISI followed by pickup model distributions shows that this signature can be seen at incident pion energies higher than 118 MeV. One of the main issues of this paper is to address the question of how much of the 3NA absorption mode in ^{4}He is ending up, via pickup, in the (ppd) channel and what fraction of it can be understood in terms of cascade+pickup ($ISI_{(ppp)n}$+pickup, $HFSI_{(ppp)n}$ +pickup) processes.

In Refs. [13,15,18] we found that a significant fraction of the three-proton cross section on ^{3}He and ^{4}He around and above the Δ resonance can be accounted for by an ISI

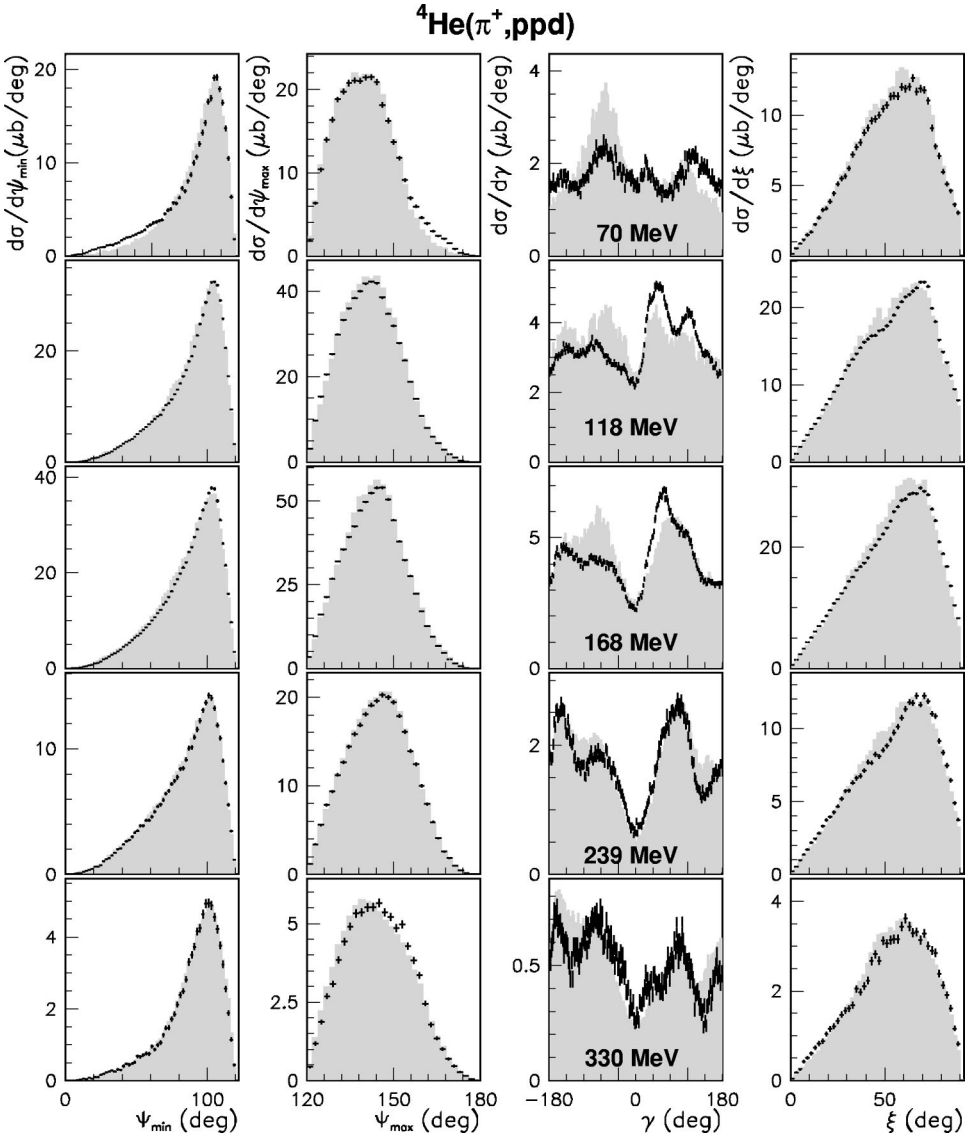

FIG. 7. Distributions of the orthogonal variables (acceptance corrected) in the selected $[ppd]$ channel. The structureless β angle is not shown. The shaded areas are the sums of the fitted simulations. For further information see Fig. 6.

mechanism followed by 2NA. It was also found that a possible contribution of a HFSI mechanism cannot be easily distinguished from a $3N$ phase space distribution, but it was observed that the HFSI yield leading to three energetic protons usually seemed to be smaller than the ISI yield. More than half of the $3p$ yield was found not to be explainable by simple cascade processes both in ^{3}He and ^{4}He. In this work a decomposition of the ppd final state was done with a simultaneous fit of seven models to the distributions of the data. The quality of the fits is illustrated in Figs. 7, 8, and 9. The fit to the orthogonal variable set is good, and also the polar angle and kinetic energy spectra are fitted well. The results of the decomposition, extrapolated to zero threshold, are given in Table III. The percentages given are average values of the results of fits to different variable sets and with different thresholds applied (see Sec. IV D). The cited uncertainties are the standard deviations of the results from the fits models. In Table IV the fractions of the multinucleon yields of the possible absorption mechanisms after pion absorption on ^{4}He are compared to the total pion absorption cross section of ^{4}He. The third open multinucleon channel ^{3}He p was not accessible to this experiment, but its yield is known to be weak (about 0.6% of the total absorption cross section at $T_\pi = 120$ MeV) [10] and therefore it is neglected here. Although the uncertainties of most of the fractions are rather large, the results show which processes are more important and also some trends in the energy dependences. One may conclude that ISI followed by pickup is able to explain significant strength of the (ppd) yield, being more important at higher incident pion energies. This result is consistent with results from our previous publications [13,15,18] where evidence for signatures of ISI in the $3p$ multinucleon channel of ^{3}He and ^{4}He was discussed extensively.

The fractions found for the HFSI+pickup mechanism indicate that this seems to be the less important cascade process. Although ISI followed by pickup is found to be important, more than half of the (ppd) yield cannot be accounted for by our semiclassical cascade models. The remainder is well fitted by simple $3N$ phase space followed by pickup distributions, if angular momentum components up to p wave are taken into account.

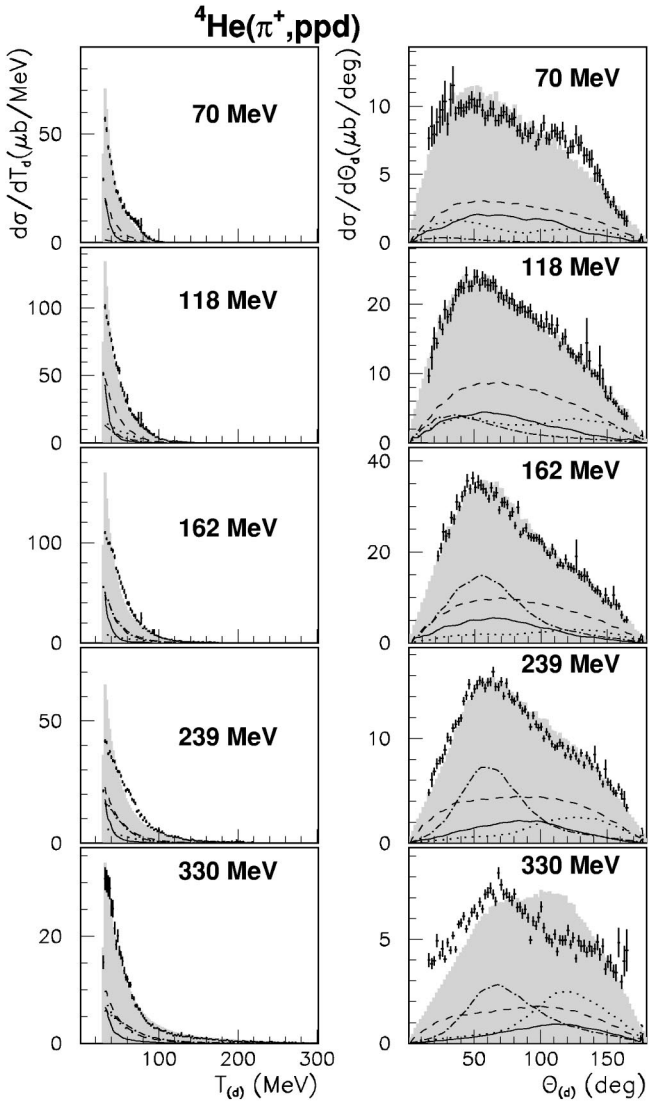

FIG. 8. The laboratory kinetic energy and polar angle distributions of the deuteron (acceptance corrected) in the selected $[ppd]$ channel. For further information see Fig. 6.

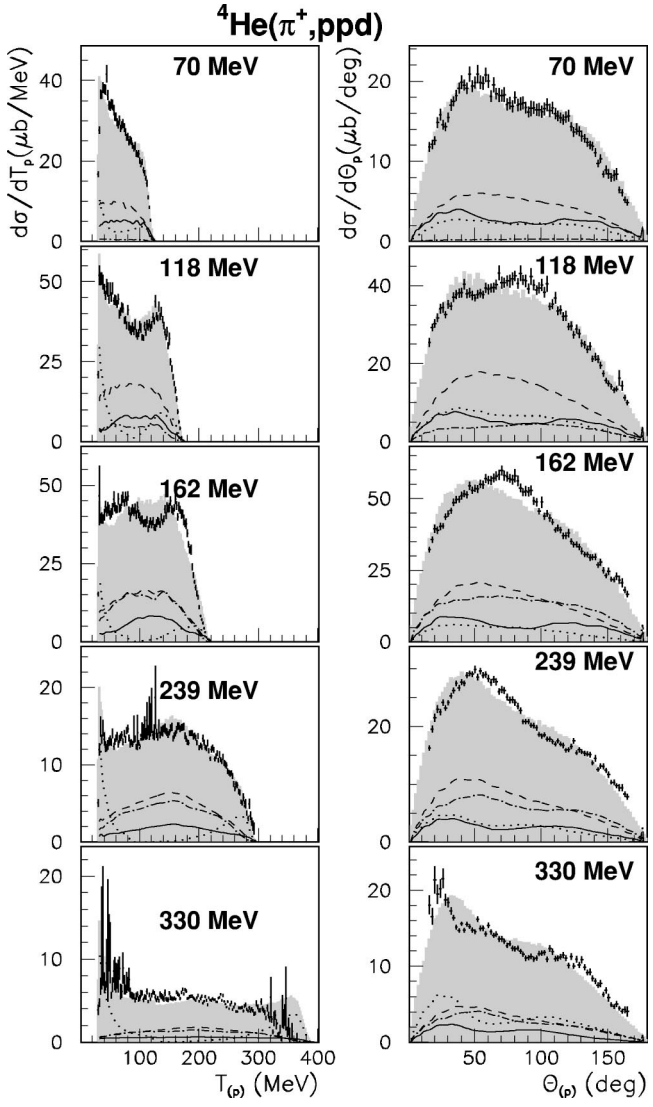

FIG. 9. The laboratory kinetic energy and polar angle distributions of the protons (acceptance corrected) in the selected $[ppd]$ channel. For further information see Fig. 6.

TABLE III. Multinucleon cross sections for the reaction $\pi^+ + {}^4\mathrm{He} \rightarrow ppd$ and their fractional decompositions into absorption mechanisms. The numbers are extrapolated to 0 MeV threshold. The errors on the fractional decompositions indicate the stability of the results under the choice of different fitting procedures. 3N-PS is the sum of the two ($3\mathrm{NA}^{L\geq 0}_{(ppp)n}$ + pickup and $3\mathrm{NA}^{L\geq 1}_{(ppp)n}$ + pickup) given 3NA channels. The cross section for the 2NA mode $[(pp)d]$ was fixed (see text).

T_π (MeV)	70	118	162	239	330
$(\mathrm{ISI}_{(ppp)n}$ + pickup)	9±5%	27±16%	46±12%	39±3%	31±7%
$(\mathrm{HFSI}_{(ppp)n}$ + pickup)	11±8%	9±15%	6±10%	0±0%	9±11%
$3\mathrm{NA}^{L\geq 0}_{(ppp)n}$ + pickup	35±9%	47±11%	24±12%	10±7%	5±7%
$3\mathrm{NA}^{L\geq 1}_{(ppp)n}$ + pickup	17±14%	8±7%	19±6%	42±4%	43±8%
$3N$-PS(ppp) + pickup	52±7%	56±10%	43±10%	52±6%	48±8%
$4N$-PS$(pppn)$ + pickup	17±14%	8±5%	5±3%	10±4%	12±7%
$\sigma_{(ppd)}$ (mb)	1.5±0.2	3.2±0.6	4.7±0.7	1.5±0.1	0.7±0.1

TABLE IV. Fractions of the multinucleon yields of the possible absorption mechanisms of the reactions $\pi^+ + {}^4\mathrm{He} \rightarrow pppn$ (taken from Ref. [18]) and $\pi^+ + {}^4\mathrm{He} \rightarrow ppd$ compared to the total pion absorption cross section of ^{4}He (taken from Ref. [17]). The given uncertainties on the individual mechanisms are those of Table III scaled appropriately. The uncertainties of the columns ''Total $pppn$'' and ''Total ppd'' are gained from the errors of the cross sections of the respective final state and those of the total absorption cross sections added in quadrature.

T_π (MeV)	70	118	162	239	330
$\sigma_{\mathrm{total}}^{\mathrm{abs}}$ (mb)	35.0±5.3	52.1±3.9	50.5±4.6	26.6±2.0	14.0±1.5
(ISI+2NA)	3±4%	1±1%	3±2%	11±3%	15±5%
(2NA+HFSI)	8±5%	6±3%	3±3%	1±1%	1±2%
$3N$-PS(ppn)	12±4%	13±3%	17±4%	15±2%	26±3%
$3N$-PS(ppp)	4±2%	6±1%	10±2%	12±3%	13±3%
$4N$-PS($pppn$)	1±1%	3±1%	4±1%	8±1%	13±3%
Total $pppn$	28±7%	29±4%	37±5%	47±5%	68±10%
(ISI+2NA+pickup)	0±1%	2±1%	4±1%	2±1%	2±1%
(2NA+HFSI+pickup)	0±1%	1±1%	1±1%	0±1%	0±1%
$3N$-PS+pickup	3±1%	3±1%	4±1%	3±1%	2±1%
$4N$-PS($pppn$)+pickup	1±1%	0±1%	0±1%	1±1%	1±1%
Total ppd	4±1%	6±1%	9±2%	6±1%	5±1%

C. Comparison with *pppn* final states

In order to see what fraction of each $pppn$ generator disappears into a ppd final state, according to our pickup model, events of the $pppn$ generators which have one final state proton and neutron with relative momentum within the step function were counted. It has been found that approximately the same fraction of events from $3N$ phase space and ISI generators (which are the most important ones) goes to the ppd final state.

In Table V, cross section ratios $ppd/(ppd+pppn)$ from the data are compared to the same ratios where the inputs are yields from the simulations. For the data with a 30 MeV threshold the ratio data/MC is roughly independent of the incident pion energy, but the normalization can vary freely. This energy independent ratio, in combination with the low ppd final state contribution to the total absorption cross section, indicates that the picture drawn from the analysis of the composition of the $pppn$ data of Ref. [18] would not be significantly modified by taking account of the influence of the deuteronic channels.

TABLE V. Data cross section ratios $ppd/(ppd+pppn)$ compared to the same ratios where inputs are yields from the MC simulations with the thresholds 30 and 0 MeV.

T_N^{thr} (MeV)	T_π (MeV)	70	118	162	239	330
0	Data	13%	17%	20%	11%	7%
0	MC	8%	6%	5%	3.5%	2.5%
30	Data	12%	10%	10%	6%	4%
30	MC	2%	1.5%	1.3%	1%	0.7%

VI. SUMMARY AND CONCLUSIONS

In this paper we have presented an analysis of the ppd final state after the absorption of a positive pion on ^{4}He for five energies across the $\Delta(1232)$ resonance. Using a complete set of five independent variables for this three particle final state and simple models, which comprise 2NA, 3NA, and 4NA models from Ref. [18] followed by pickup, the yield was investigated for contributions from the cascade mechanisms where the basic 2NA process is accompanied by initial or final state interactions plus pickup. The cross sections of the (ppd) and $(pd)p$ physics channels were evaluated. For the first time an estimate of the total absorption cross section at 330 MeV of pion incident energy is given.

The distributions of the selected $[pd]$ channel are consistent with absorption on a quasideuteron pair, followed by the pickup of a neutron by one of the outgoing protons, although an alternative approach where the pion is absorbed on a quasitriton $^3\mathrm{H}(\pi^+,pd)$ with one proton acting as a spectator also gives a good description of the data. Fits to the data suggest that a significant fraction of the (ppd) yield can be described by a semiclassical (ISI+2NA+pickup) cascade model. The data do not reveal distinct kinematic signatures as suggested for a similar (2NA+HFSI+pickup) cascade process. However, our investigations of the differential cross sections suggest that these ISI and HFSI cascade mechanisms, approximated by semiclassical models, can account for less than half of the (ppd) yield, similarly to the analysis of the $pppn$ channel. The issue of whether the large non-2NA yield can be explained only by sequential processes remains unresolved. In order to understand the substantial multinucleon absorption yield, it remains imperative to have a realistic calculation of 3NA.

ACKNOWLEDGMENTS

We thank the technical staff of the Paul Scherrer Institute for the support provided to this experiment. We also thank M. Locher for useful discussions. This work was supported in part by the German Bundesministerium für Forschung und Technologie (BMFT), the German Internationales Büro der Kernforschungsanlage Jülich, the Swiss National Science Foundation, the U.S. Department of Energy (DOE), and the U.S. National Science Foundation (NSF).

[1] G. Backenstoss, M. Izycki, P. Salvisberg, M. Steinacher, P. Weber, H.J. Weyer, S. Cierjacks, S. Ljungfelt, H. Ullrich, M. Furić, and T. Petković, Phys. Rev. Lett. **55**, 2782 (1985).

[2] K.A. Aniol, A. Altman, R.R. Johnson, H.W. Roser, R. Tacik, U. Wienands, D. Ashery, J. Alster, M.A. Moinester, E. Piasetzky, D.R. Gill, and J. Vincent, Phys. Rev. C **33**, 1714 (1986).

[3] L.C. Smith, R.C. Minehart, D. Ashery, E. Piasetsky, M. Moinester, I. Navon, D.F. Geesaman, J.P. Schiffer, G. Stephens, B. Zeidman, S. Levinson, S. Mukhopadhyay, R.E. Segel, B. Anderson, R. Madey, J. Watson, and R.R. Whitney, Phys. Rev. C **40**, 1347 (1989).

[4] P. Weber, G. Backenstoss, M. Izycki, R.J. Powers, P. Salvisberg, M. Steinacher, H.J. Weyer, S. Cierjacks, A. Hoffart, B. Rzehorz, H. Ullrich, D. Bosnar, M. Furić, T. Petković, and N. Šimičević, Nucl. Phys. **A534**, 541 (1991).

[5] S. Mukhopadhyay, S. Levenson, R.E. Segel, G. Garino, D. Geesaman, J.P. Schiffer, G. Stephans, B. Zeidman, E. Ungricht, H. Jackson, R. Kowalczyk, D. Ashery, E. Piasetsky, M. Moinester, I. Navon, L.C. Smith, R.C. Minehart, G.S. Das, R.R. Whitney, R. Mckeown, B. Anderson, R. Madey, and J. Watson, Phys. Rev. C **43**, 957 (1991).

[6] P. Weber, G. Backenstoss, M. Izycki, R.J. Powers, P. Salvisberg, M. Steinacher, H.J. Weyer, S. Cierjacks, A. Hoffart, H. Ullrich, M. Furić, T. Petković, and N. Šimičević, Nucl. Phys. **A501**, 765 (1989).

[7] P. Salvisberg, G. Backenstoss, H. Krause, R.J. Powers, M. Steinacher, H.J. Weyer, M. Wildi, A. Hoffart, B. Rzehorz, H. Ullrich, D. Bosnar, M. Furić, T. Petković, N. Šimičević, H. Zmeskal, A. Janett, and R.H. Sherman, Phys. Rev. C **46**, 2172 (1992).

[8] T. Alteholz, D. Androić, G. Backenstoss, D. Bosnar, H. Breuer, A. Brković, H. Döbbeling, T. Dooling, W. Fong, M. Furić, P.A.M. Gram, N.K. Gregory, J.P. Haas, A. Hoffart, C.H.Q. Ingram, A. Klein, K. Koch, J. Köhler, B. Kotliński, M. Kroedel, G. Kyle, A. Lehmann, Z.N. Lin, G. Mahl, A.O. Mateos, K. Michaelian, S. Mukhopadhyay, T. Petković, R.P. Redwine, D. Rowntree, R. Schumacher, U. Sennhauser, N. Šimičević, F.D. Smit, G. van der Steenhoven, D.R. Tieger, R. Trezeciak, H. Ullrich, M. Wang, M.H. Wang, H.J. Weyer, M. Wildi, and K.E. Wilson, Phys. Rev. Lett. **73**, 1336 (1994).

[9] H. Hahn, A. Altman, D. Ashery, G. Gefen, D.R. Gill, R.R. Johnson, R. Levy-Nathansohn, M.A. Moinester, M. Sevior, and R.P. Trelle, Phys. Rev. C **53**, 1074 (1996).

[10] M. Steinacher, G. Backenstoss, M. Izycki, P. Salvisberg, P. Weber, H.J. Weyer, A. Hoffart, B. Rzehorz, H. Ullrich, M. Dzemidzić, M. Furić, and T. Petković, Nucl. Phys. **A517**, 413 (1990).

[11] P. Weber, J. McAlister, R. Olszewski, A. Feltham, M. Hanna, R. Johnson, M. Pavan, C. Ponting, F. Rozon, M. Sevior, V. Sossi, D. Vetterli, D. Humphrey, G. Lolos, Z. Papandreou, R. Tacik, D. Ottewell, G. Sheffer, G. Smith, Y. Mardor, and S. May-Tal, Phys. Rev. C **43**, 1553 (1991).

[12] G. Backenstoss, M. Izycki, R. Powers, P. Salvisberg, M. Steinacher, P. Weber, H.J. Weyer, A. Hoffart, B. Rzehorz, H. Ullrich, D. Bosnar, M. Furić, and T. Petković, Phys. Lett. B **222**, 7 (1989).

[13] G. Backenstoss, D. Bosnar, H. Breuer, H. Döbbeling, T. Dooling, M. Furić, P.A.M. Gram, N.K. Gregory, A. Hoffart, C.H.Q. Ingram, A. Klein, K. Koch, J. Köhler, B. Kotliński, M. Kroedel, G. Kyle, A. Lehmann, A.O. Mateos, K. Michaelian, T. Petković, R.P. Redwine, D. Rowntree, U. Sennhauser, N. Šimičević, R. Trezeciak, H. Ullrich, M. Wang, M.H. Wang, H.J. Weyer, M. Wildi, and K.E. Wilson, Phys. Lett. B **379**, 60 (1996).

[14] D. Androić, G. Backenstoss, D. Bosnar, H. Breuer, H. Döbbeling, T. Dooling, M. Furić, P.A.M. Gram, N.K. Gregory, A. Hoffart, C.H.Q. Ingram, A. Klein, K. Koch, J. Köhler, B. Kotliński, M. Kroedel, G. Kyle, A. Lehmann, A.O. Mateos, K. Michaelian, T. Petković, R.P. Redwine, D. Rowntree, U. Sennhauser, N. Šimičević, R. Trezeciak, H. Ullrich, M. Wang, M.H. Wang, H.J. Weyer, M. Wildi, and K.E. Wilson, Phys. Rev. C **53**, R2591 (1996).

[15] A. Lehmann, D. Androić, G. Backenstoss, D. Bosnar, H. Breuer, H. Döbbeling, T. Dooling, M. Furić, P.A.M. Gram, N.K. Gregory, A. Hoffart, C.H.Q. Ingram, A. Klein, K. Koch, J. Köhler, B. Kotliński, M. Kroedel, G. Kyle, A.O. Mateos, K. Michaelian, T. Petković, M. Planinić, R.P. Redwine, D. Rowntree, U. Sennhauser, N. Šimičević, R. Trezeciak, H. Ullrich, M. Wang, M.H. Wang, H.J. Weyer, M. Wildi, and K.E. Wilson, Phys. Rev. C **55**, 2931 (1997).

[16] H. Kamada, M.P. Locher, T.-S.H. Lee, J. Golak, V.E. Markushin, W. Glöckle, and H. Witala, Phys. Rev. C **55**, 2563 (1997).

[17] A.O. Mateos, D. Androić, G. Backenstoss, D. Bosnar, H. Breuer, H. Döbbeling, T. Dooling, M. Furić, P.A.M. Gram, N.K. Gregory, A. Hoffart, C.H.Q. Ingram, A. Klein, K. Koch, J. Köhler, B. Kotliński, M. Kroedel, G. Kyle, A. Lehmann, K. Michaelian, T. Petković, M. Planinić, R.P. Redwine, D. Rowntree, U. Sennhauser, N. Šimičević, R. Trezeciak, H. Ullrich, M. Wang, M.H. Wang, H.J. Weyer, M. Wildi, and K.E. Wilson, Phys. Rev. C **58**, 942 (1998).

[18] A. Lehmann, D. Androić, G. Backenstoss, D. Bosnar, H. Breuer, H. Döbbeling, T. Dooling, M. Furić, P.A.M. Gram, N.K. Gregory, A. Hoffart, C.H.Q. Ingram, A. Klein, K. Koch, J. Köhler, B. Kotliński, M. Kroedel, G. Kyle, A.O. Mateos, K. Michaelian, T. Petković, M. Planinić, R.P. Redwine, D. Rowntree, U. Sennhauser, N. Šimičević, R. Trezeciak, H. Ullrich, M. Wang, M.H. Wang, H.J. Weyer, M. Wildi, and K.E. Wilson, Phys. Rev. C **56**, 1872 (1997).

[19] W.R. Wharton, P.D. Barnes, B. Bassalleck, R.A. Eisenstein, G.

Franklin, R. Grace, C. Maher, P. Pile, R. Rieder, J. Szymanski, F. Takeutchi, J.F. Amann, S.A. Dytman, and K.G.R. Doss, Phys. Rev. C **33**, 1435 (1986).

[20] G. Backenstoss, H. Breuer, H. Döbbeling, M. Furić, P.A. Gram, A. Hoffart, C.H.Q. Ingram, A. Klein, B. Kotliński, G.S. Kyle, K. Michaelian, S. Mukhopadhyay, T. Petković, R.P. Redwine, D. Rowntree, R.A. Schumacher, U. Sennhauser, N. Šimičević, F.D. Smit, G. van der Steenhoven, D.R. Tieger, H. Ullrich, M.H. Wang, H.J. Weyer, M. Wildi, and K.E. Wilson, Nucl. Instrum. Methods Phys. Res. A **310**, 518 (1991).

[21] T. Alteholz, D. Androić, G. Backenstoss, D. Bosnar, H. Breuer, A. Brković, H. Döbbeling, T. Dooling, W. Fong, M. Furić, P.A.M. Gram, N.K. Gregory, J.P. Haas, A. Hoffart, C.H.Q. Ingram, A. Klein, K. Koch, J. Köhler, B. Kotliński, M. Kroedel, G. Kyle, A. Lehmann, Z.N. Lin, G. Mahl, A.O. Mateos, K. Michaelian, S. Mukhopadhyay, T. Petković, M. Planinić, R.P. Redwine, D. Rowntree, R. Schumacher, U. Sennhauser, N. Šimičević, F.D. Smit, G. van der Steenhoven, D.R. Tieger, R. Trezeciak, H. Ullrich, M. Wang, M.H. Wang, H.J. Weyer, M. Wildi, and K.E. Wilson, Nucl. Instrum. Methods Phys. Res. A **373**, 374 (1996).

[22] D. Rowntree, D. Androić, G. Backenstoss, D. Bosnar, H. Breuer, T. Dooling, M. Furić, P.A.M. Gram, N.K. Gregory, A. Hoffart, C.H.Q. Ingram, A. Klein, K. Koch, J. Köhler, B. Kotlinski, M. Kroedel, G. Kyle, A. Lehmann, A.O. Mateos, K. Michaelian, T. Petković, M. Planinić, R.P. Redwine, N. Šimičević, R. Trezeciak, H.J. Weyer, M. Wildi, and K.E. Wilson, Phys. Rev. C **60**, 054610 (1999).

[23] R. Trezeciak, Ph.D. thesis, University of Karlsruhe, 1995.

[24] K. Wilson, Ph.D. thesis, MIT Cambridge, 1995.

[25] B.G. Ritchie, Phys. Rev. C **44**, 533 (1991).

[26] R. Schiavilla, V.R. Pandharipande, and R.B. Wiringa, Nucl. Phys. **A449**, 219 (1986).

[27] J.F.J. van den Brand, H.P. Blok, R. Ent, E. Jans, J.M. Laget, L. Lapikás, C. de Vries, and P.K.A. de Witt Huberts, Nucl. Phys. **A534**, 637 (1991).

[28] N. Šimičević and A. Mateos, Phys. Rev. C **51**, 797 (1995).

[29] SCATPI, J.B. Walter, and G.A. Rebka, Los Alamos National Laboratory Report No. LA-7731-MS, 1979.

[30] R.A. Arndt, L.D. Roper, R.A. Bryan, R.B. Clark, B.J. VerWest, and P. Signell, Phys. Rev. D **28**, 97 (1983); R.A. Arndt, L.D. Roper, R.L. Workman, and M.W. McNaughton, *ibid.* **45**, 3995 (1992); SAID, R.A. Arndt *et al.*, Virginia Polytechnic Institute, 1988.

[31] P. Marmier and E. Sheldon, *Physics of Nuclei and Particles* (Academic, New York, 1969), pp. 882–905.

[32] L. Salcedo, E. Oset, and D. Strottman, Phys. Lett. B **208**, 339 (1988).

[33] M. Planinić, Ph.D. thesis, University of Zagreb, 1999.